


Nonlinear ion mobility at high electric field strengths in the perovskites SrTiO₃ and CH₃NH₃PbI₃Dennis Kemp and Roger A. De Souza ^{*}*Institute of Physical Chemistry, RWTH Aachen University, 52056 Aachen, Germany* (Received 25 June 2021; revised 11 August 2021; accepted 21 September 2021; published 5 October 2021)

As the characteristic dimensions of perovskite devices shrink to the nanoscale, operating voltages of a few volts lead to huge field strengths and, consequently, to the possibility of field-enhanced ion mobility. In this paper, the electrochemical mobility of X anions (u_X) along $\langle 100 \rangle$ in the ABX_3 perovskite structure was investigated as a function of electric field strength E and temperature T by means of classical molecular dynamics simulations. Two different cases were examined: one representative of inorganic perovskites, oxide-ion mobility (u_O) in cubic SrTiO₃; and the other representative of hybrid inorganic-organic perovskites, iodide-ion mobility (u_I) in cubic CH₃NH₃PbI₃. In both cases, isothermal mobilities are, as expected, independent of field at low values ($E < 10^0$ MV cm⁻¹) but become field dependent at higher values. Data obtained for $u_O(E, T)$ can be described quantitatively with an analytical treatment incorporating a modified Haven ratio for a dilute solution. In contrast, $u_I(E, T)$ displays complex behavior. At high fields, the degree of field enhancement is underestimated by the analytical treatment, while in the field-independent regime, the data imply that moderate fields decrease u_I . Our study thus demonstrates that for cubic, inorganic ABX_3 perovskites $u_X(E, T)$ along $\langle 100 \rangle$ can now be predicted quantitatively, but for hybrid perovskites substantially more complex models are required.

DOI: [10.1103/PhysRevMaterials.5.105401](https://doi.org/10.1103/PhysRevMaterials.5.105401)

I. INTRODUCTION

Various materials with the ABX_3 perovskite structure display properties whose utilization requires the application of a voltage. For example, BaTiO₃ exhibits high dielectric permittivity, which leads to its use as a dielectric in multilayer ceramic capacitors [1,2]; BiFeO₃ is a multiferroic material, with applications in magnetic and spintronic devices [3,4]; CH₃NH₃PbI₃ shows outstanding optoelectronic properties that are used in photovoltaic devices [5–7]; (La, Sr)(Ga, Mg)O₃ and (Na, Bi)(Ti, Mg)O₃ display high oxide-ion conductivity and negligible electronic conductivity over a wide range of conditions and are considered electrolytes for solid oxide fuel cells [8]; and SrTiO₃'s structural simplicity, chemical stability and thorough characterisation make it a model perovskite, in particular for valence-change resistive switching devices [9,10].

Applying a voltage to a perovskite will unavoidably lead to the drift of all charge carriers, be they electronic or ionic in nature. In some of the cases mentioned above (fuel cells, resistive switches), the drift of the ionic charge carriers is central to the application, whereas in others (dielectrics, photovoltaics) it is detrimental to device performance. Given that such devices are generally operated under voltages of the order of a few volts, device dimensions of the order of tens or hundreds of nanometers automatically translate into electric field strengths of the order of MV cm⁻¹. At such enormous values, the field can increase exponentially the ions' drift velocity [11–13]. This behavior can be beneficial or detrimental, as already noted by Roling *et al.* [14]: Materials displaying

low mobilities at low fields can be employed as electrolytes at high fields because of the field-induced enhancement. Dielectric materials, on the other hand, will suffer from ions that are hardly mobile under normal conditions, becoming substantially more mobile at high fields.

All theoretical treatments so far consider the migrating ion to jump along a straight path between initial and final configurations, with the field applied in the same direction, i.e., the migration vector and the field vector are collinear [11–13,15–17]. This is not the case, however, for the migration of X anions by a vacancy mechanism in an ABX_3 perovskite because migration occurs along a curved path between anion sites adjacent along $\langle 110 \rangle$ [see Fig. 1] [18–23]. In this paper, we employed classical molecular dynamics (MD) simulations to examine the field-enhanced mobility of anions in two perovskites.

The two perovskites we studied were SrTiO₃ and CH₃NH₃PbI₃ (MAPbI₃), and we investigated ion migration along $\langle 100 \rangle$ of the cubic perovskite unit cell, since the most common orientation of perovskite devices is $\langle 100 \rangle$. SrTiO₃ was chosen for three reasons: anion migration in the absence of fields is well understood both experimentally and computationally [24–30], and hence this material serves as a reference for more complex systems; it is, as mentioned above, a model material for resistive switching, a phenomenon for which the ion mobility at high fields is an important issue [31]; and field-accelerated oxygen-ion transport has been examined experimentally [32–34] but there are substantial discrepancies between these studies and a coherent picture is missing. MAPbI₃ was also chosen for three reasons: it is a prototypical hybrid organic–inorganic perovskite; its ion transport properties and defect chemistry, though not entirely understood, are the best characterized among the hybrid perovskites [35–40];

^{*}desouza@pc.rwth-aachen.de

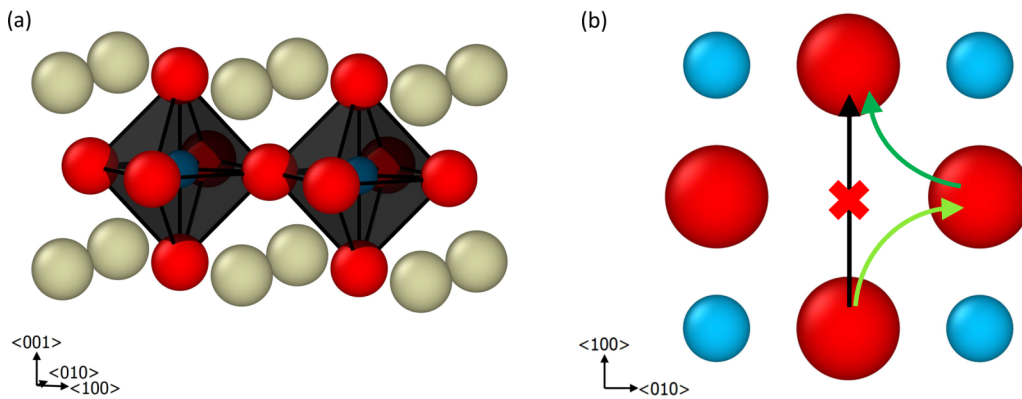


FIG. 1. (a) Crystal structure of the cubic perovskite SrTiO₃. The Ti cations (blue) are sixfold coordinated by oxygen anions (red) and occupy the octahedral interstices of the simple cubic sublattice of Sr cations (grey). (b) Schematic illustration of oxygen-ion migration for a field applied in $\langle 100 \rangle$: Transport occurs (see text) by two consecutive curved paths (light and dark green arrows) along $\langle 110 \rangle$, rather than directly along $\langle 100 \rangle$ (black arrow). When additionally an electric field is applied in $\langle 100 \rangle$, the two consecutive jumps along $\langle 110 \rangle$ become nonequivalent. All crystal structures in this document are created with the software package OVITO [43].

and in terms of field-driven ion transport, it represents a rather complicated case because of the methylammonium cations (MA⁺), which rotate on their lattice sites in the cubic structure and possess a dipole whose interaction with the applied field will affect ion migration. Such effects may generate an additional source of nonlinearity that is necessary for the resistive switching phenomenon [41].

We performed classical MD simulations, as opposed to experiments, for three particular reasons. First, in experimental studies of high-field ion mobility, one is confronted with a variety of alternative sources of nonlinear behavior [16,42], such as interfacial processes at grain boundaries and electrodes, temperature increases arising from Joule heating, electronic transport, stoichiometry polarization, and sample decomposition. In classical MD simulations, such problems are either easily avoided or easily identified. Second, MD simulations offer complete control of the system under investigation, especially in terms of the number and type of ionic charge carriers present. In this way, they provide transport data that not only refer unambiguously to the movement of a specific charge carrier but also are free from the effects of interactions with other types of charge carriers, if so required. Experiments, in contrast, may be complicated by various charge carriers being present, including electronic charge carriers, and doubts may arise as to which charge carrier is being examined or as to whether charge-carrier interactions are important. Third, atomistic simulations allow insights into the transport behavior on the atomistic scale. We utilized these benefits of MD simulations to examine if the complex case of ion mobility in perovskites can be described with an analytical expression. Our primary aim is to establish for this transport phenomenon in these materials a firm, quantitative foundation.

II. THEORY

We summarize first in Sec. II A the basics of field-driven ion transport [11–13], after which we focus on a recent quantitative treatment [16]. In Sec. II B, we examine the link between ion mobility and tracer diffusivity and obtain a surprising result for the Haven ratio. Subsequently, we discuss

in detail some expected peculiarities of field-driven anion transport in the ABX₃ perovskite structure in Sec. II C.

A. The drift velocity of ions in an electric field

The effect of an electric field on ion transport in a solid was first considered by Verwey [11], Frenkel [12], and Mott and Gurney [13]. Independently, they obtained, for an ion of charge $z_i e$ migrating between sites separated by a distance d_i at temperature T , a hyperbolic sine dependence of the ions' drift velocity on the applied field (k_B is Boltzmann's constant):

$$v_{d,i} \propto \sinh \left(\frac{|z_i| e E d_i}{2k_B T} \right). \quad (1)$$

At low fields, or more correctly, for $|z_i| e E d_i \ll 2k_B T$, the sinh term can be replaced by its argument ($\sinh x \approx x$ for $x \ll 1$) and a linear relation between drift velocity and field strength results (the constant of proportionality being the mobility u_i). In contrast, at high fields, $E > (2k_B T)/(|z_i| e d_i)$, an exponential increase in drift velocity with increasing field strength is expected, since $\sinh x \approx e^x/2$ for $x \gg 1$, and u_i becomes field dependent. While qualitatively correct, Eq. (1) overestimates the increase in drift velocity at high fields [15,16]. An improved expression was recently derived by taking into account the shape of the potential energy landscape in which the ion migrates [16]. Starting with a cosinusoidal energy profile upon which a linear field is superimposed,

$$H_{\text{mig}}(x) = \frac{\Delta H_{\text{mig}}}{2} \left[1 - \cos \left(\frac{2\pi x}{d_i} \right) \right] - |z_i| e E x, \quad (2)$$

where x is the migration coordinate and ΔH_{mig} is the activation enthalpy at zero field, one obtains that the activation enthalpies for jumps in the forward and reverse directions are

$$\Delta H_{\text{mig}}^{\text{fr}} = \Delta H_{\text{mig}} \left[\sqrt{1 - \gamma^2} \mp \gamma \left(\frac{\pi}{2} \right) + \gamma \arcsin \gamma \right], \quad (3)$$

with $\gamma = (|z_i|eEd_i)/(\pi \Delta H_{\text{mig}})$. The ions' drift velocity is thus

$$v_{d,i} = n_v d_i v_0 \exp\left(\frac{\Delta S_{\text{mig}}}{k_B}\right) \times \left[\exp\left(-\frac{\Delta H_{\text{mig}}^f}{k_B T}\right) - \exp\left(-\frac{\Delta H_{\text{mig}}^r}{k_B T}\right) \right], \quad (4)$$

where n_v is the site fraction of vacant sites; v_0 is the attempt frequency and ΔS_{mig} is the activation entropy of migration. This approach yields a quantitative description of oxide-ion mobility in CeO_2 over a wide range of field strengths [16].

B. The link between tracer diffusivity and ion mobility

As mentioned above, the ion mobility u_i is defined as the constant of proportionality between v_d and E :

$$v_d = u_i E. \quad (5)$$

In the low-field limit, $E \ll (2k_B T)/(|z_i|ed_i)$, one thus obtains from Eqs. (3) and (4)

$$\lim_{E \rightarrow 0} u_i = n_v d_i^2 \frac{|z_i|e}{k_B T} v_0 \exp\left(\frac{\Delta S_{\text{mig}}}{k_B}\right) \exp\left(-\frac{\Delta H_{\text{mig}}}{k_B T}\right). \quad (6)$$

Alternatively [44,45], one can obtain u_i from D_i^* (the tracer diffusivity of i) via D_i^σ (the conductivity diffusion coefficient) by combining the Nernst–Einstein equation

$$u_i = D_i^\sigma \frac{|z_i|e}{k_B T} \quad (7)$$

and the Haven ratio

$$H_r = \frac{D_i^*}{D_i^\sigma}. \quad (8)$$

From random-walk theory, one can express the tracer diffusivity as

$$D_i^* = f^* n_v \frac{Z}{6} d_i^2 v_0 \exp\left(\frac{\Delta S_{\text{mig}}}{k_B}\right) \exp\left(-\frac{\Delta H_{\text{mig}}}{k_B T}\right), \quad (9)$$

where f^* is the tracer correlation factor (which for the migration of noninteracting anion vacancies in a cubic perovskite is given by $f^* = 0.69$ [46]). Combining Eqs. (7)–(9) and comparing the result with Eq. (6), we find that the Haven ratio does not take the expected value of f^* for a dilute solution of noninteracting defects, but $f^*(Z/6)$. Expressing H_r as the ratio of tracer and conductivity correlation coefficients ($= f^*/f^\sigma$), we conclude that this approach yields $f^\sigma = 6/Z$. In the past (see, e.g., Ref. [47]), this sort of approach focused on the general form of the relationship, and in particular on its temperature dependence; scant attention was paid to the exact form of the pre-exponential term. The simulation data that we obtain require the exact form to be specified.

The main result for the present study is that suitable tracer diffusion data can be used to predict the low-field u_i with Eqs. (7) and (8), and subsequently, $u_i(E, T)$ with Eqs. (3)–(5), as long as certain conditions are met (in particular, collinear migration and field vectors, and a sinusoidal energy barrier). This does not necessarily seem to be the case for anion migration in perovskites, however, as discussed below.

C. Anion migration in the perovskite structure

As noted in Sec. I, anion-vacancy migration along $\langle 110 \rangle$ constitutes a complex case because the trajectory of the migrating anion is curved, as depicted in Fig. 1(b). This means that the contribution of the field, regardless of its direction, varies at every point during the jump. There is also the possibility of the field altering the trajectories of the migrating anions, making the path more or less curved. Additionally, for a field applied along $\langle 100 \rangle$, the two (symmetry-equivalent) jumps that together yield transport along $\langle 100 \rangle$ become inequivalent because the contribution of the field in the jump directions are principally different: For the first jump in Fig. 1(b), the ion starts parallel to the field vector, whereas for the second jump it starts perpendicular to it.

These issues mean that, strictly speaking, the treatment in Sec. II A is not valid. One could try to take account of these issues by introducing a variable field contribution that modifies the energy landscape locally and by incorporating the inequality of the jumps arising from their different orientations toward the field vector. Anticipating later results, however, we propose to ignore the curvature of the migration paths and to ignore the two inequivalent migration jumps. Consequently, in using Eq. (3) we assume a single barrier that is modified by $E \cos(\pi/4)$, representing the angle between field vector and migration vector for both jumps.

Although the nearest-neighbor jump of an anion into a vacant site takes place along $\langle 110 \rangle$ in the ABX_3 perovskite structure, as illustrated in Fig. 1(b), the anion jump to a next nearest-neighbor vacancy along $\langle 100 \rangle$ seems at first sight worthy of consideration, given that the field is applied along $\langle 100 \rangle$. Closer examination, however, suggests that the latter path will have a prohibitively high activation barrier, since it involves the migrating anion directly passing two other anions (rather than just 2 A cations and 1 B cation as for $\langle 110 \rangle$ jumps) and it will thus be characterized by increased Coulomb repulsion [48,49]. Indeed, for oxygen-vacancy migration in SrTiO_3 , atomistic simulations confirm that the latter path has a prohibitively high activation barrier, $\Delta H_{\text{mig}}^{(100)} \approx 4$ eV compared with $\Delta H_{\text{mig}}^{(110)} = 0.62$ eV [48]. Anion jumps along $\langle 100 \rangle$ in the cubic ABX_3 perovskite structure can therefore be neglected.

Finally, we note that acceptor-type species, such as dopant cations and cation vacancies, are well known to interact with anion vacancies, trapping them in defect associates and increasing their barriers for migration [27,50–52]. For this reason, the simulation cells contained only dilute solutions of anion vacancies (and no acceptor species) so all defect–defect interactions can be safely ignored.

III. SIMULATIONS

A. Choice of method

Classical MD simulations that employed empirical pair potentials (EPPs) were used to obtain $u_i(E, T)$. Our decision to use classical MD simulations was guided primarily by two requirements. First, the electrochemical mobilities should be obtained directly from the simulations without excessive computational expense. An alternative procedure to MD is to combine density-functional theory (DFT) calculations of ΔS_{mig} and ΔH_{mig} with kinetic Monte Carlo

simulations [53–55]. In the present case, that would involve determining $\Delta S_{\text{mig}}(E, T)$ and $\Delta H_{\text{mig}}(E, T)$. DFT calculations of $\Delta S_{\text{mig}}(T)$ alone represent an enormous computational expense [54]. The second requirement is that the experimental behavior of defect migration is reproduced in the simulations. We showed previously that the set of EPPs from Pedone *et al.* [56] perform exceedingly well for oxygen-vacancy migration in SrTiO₃ [28,48] (and also in BaTiO₃ [57]) and that the MYP set of EPPs [58,59] perform exceedingly well for iodine-vacancy and iodine-interstitial migration in MAPbI₃ [37,38,60,61]. In addition, the MYP set of EPPs also captures the rotation of the MA⁺ cations [58]. Together, these two requirements lead to the use of classical MD simulations.

One may be concerned about electrons not being included in the simulations, the ions in both cases being treated as classical charged particles. In particular, the effect of a field on the electron distribution could conceivably produce changes in the barriers over which ions jump. We contend that the inclusion of electrons is unnecessary for all but the very highest fields, and we provide an argument and evidence in support below. Our line of reasoning is based on the relevant energy scale.

In a solid, electrons have much higher thermal energies than ions by 1 to 2 orders of magnitude. Let us consider, from Eq. (1), $k_{\text{B}}T = E|z_i|ed_i/2$ as equating thermal energy with the energy supplied by the field in moving a charge a distance $d_i/2$. Since this relation is linear, the field required to affect the motion of electrons will be one to two orders of magnitude higher than those required to affect the ions. This argument, though very simple, is supported by DFT studies [62,63] in which field strengths of (25 to 200) MV cm⁻¹ are required to affect the binding energies of molecules, i.e., one to two orders of magnitude higher than those required to affect ionic motion at 1000 K. (There is also support from experiments, see Refs. [64–66]). Thus, to a first approximation, we can examine the effects of an electric field on ion migration in a solid without having to include electrons explicitly in the simulations.

In further support of our argument, we mention DFT calculations [67] of ion migration in MgO, in which activation barriers for ion migration are modified by field strengths of $>10^0$ MV cm⁻¹. This result is exactly in line with the classical treatment [11–13,16], indicating that taking electrons into account does not change the physics of the migration process.

B. Simulation details

We performed MD simulations using the LAMMPS code [68] with periodic boundary conditions in the NpT ensemble (constant particle number N , constant pressure p , and constant temperature T). For SrTiO₃, the long-range Coulombic interactions were evaluated by an Ewald summation [69] with an accuracy of 10^{-6} , for MAPbI₃ they were evaluated with a particle-particle particle-mesh solver [70] with an accuracy of 10^{-5} . In both cases, the velocity Verlet algorithm was used for solving the equations of motion with a time step of 1 fs. Temperature (pressure) of both systems were controlled by Nosé–Hoover thermostat (barostat) [71,72], with damping parameters 2 ps (50 ps) for SrTiO₃ and 0.2 ps (20 ps) for MAPbI₃.

Oxygen transport in SrTiO₃ was examined in a supercell containing 34 295 ions (6859 f.u., Sr₆₈₅₉Ti₆₈₅₉O₂₀₅₇₇); for

iodine transport in MAPbI₃, a supercell with 48 000 ions [4000 f.u., (CH₃NH₃)₄₀₀₀Pb₄₀₀₀I₁₂₀₀₀] was employed. An anion vacancy site fraction of $n_v = 0.4\%$ was introduced in each system by randomly removing 82 oxygen ions or 48 iodine ions, and the missing charge was compensated by lowering the charge of the Ti or Pb cations. This procedure was previously shown to be physically reasonable [16,28].

Note: The fields strengths used in the MD simulations are insufficient to generate vacancy-interstitial anion pairs, according to the thermodynamic model of Schie *et al.* [73] on the basis of anti-Frenkel Gibbs energies [38]. No evidence of such defect formation was observed in any MD simulation. This means that the defect populations are constant during the simulations and are given by the number of missing anions.

Ion mobilities were determined as a function of electric field \mathbf{E} by applying an additional force $\mathbf{F} = z_i e \mathbf{E}$ to every ion in the simulation cell and monitoring the mean displacements $|\langle r_i \rangle|$ of the anions in the field direction. If $|\langle r_i \rangle|$ increased linearly with time t , a drift velocity was determined according to $v_{d,i} = d|\langle r_i \rangle|/dt$, from which the ion mobility was then calculated with Eq. (5). In the case of SrTiO₃, mobilities were obtained for $0.5 \leq E/\text{MV cm}^{-1} \leq 35$ and for MAPbI₃, for $0.3 \leq E/\text{MV cm}^{-1} \leq 7$. At higher fields, the structures became unstable, consistent with Eq. (3) predicting $\Delta H_{\text{mig}}^{\ddagger}$ going to zero at the respective field strength; whereas at lower fields, the data quality was insufficient (as indicated, for example, by $|\langle r_i \rangle|$ not increasing linearly with t).

Both sets of EPP are characterized by partial ionic charges ($z_{\text{O}} = -1.2$, $z_{\text{I}} = -1.13$) [56,59] and this needs to be taken into account in two ways. The first issue is the ion mobility and here we first calculated the mechanical mobility $B_{m,i}$ of ion i , which is independent of z_i , and then u_i corresponding to the nominal charge z_i^{nom} :

$$B_{m,i} = \frac{v_{d,i}}{|z_i|eE}, \quad (10)$$

$$u_i = z_i^{\text{nom}} e B_{m,i}. \quad (11)$$

The second issue is the field strength that the ions perceive, and here we calculated a nominal field strength according to

$$E_{\text{nom}} = \frac{F}{z_i^{\text{nom}} e}. \quad (12)$$

IV. RESULTS AND DISCUSSION

A. Strontium titanate (SrTiO₃)

1. Field-dependent oxygen-ion mobilities

In Fig. 2(a), we plot the oxygen-ion mobilities, u_{O} , obtained from the MD simulations as a function of the nominal electric field strength E_{nom} at five different temperatures. Isothermal values of u_{O} are constant up to $E_{\text{nom}} \approx 3$ MV cm⁻¹ at these temperatures but increase strongly at higher field strengths. The individual data sets also get closer together with increasing field from $E_{\text{nom}} \approx 3$ MV cm⁻¹ onward, indicating that the temperature dependence weakens; in other words, the effective activation enthalpy, $\Delta H_{\text{eff,O}} = -k_{\text{B}}[d \ln(u_{\text{O}}T)/d(1/T)]$, decreases with increasing field strength in the nonlinear regime, as shown in Fig. 2(b). This behavior is qualitatively consistent with the standard

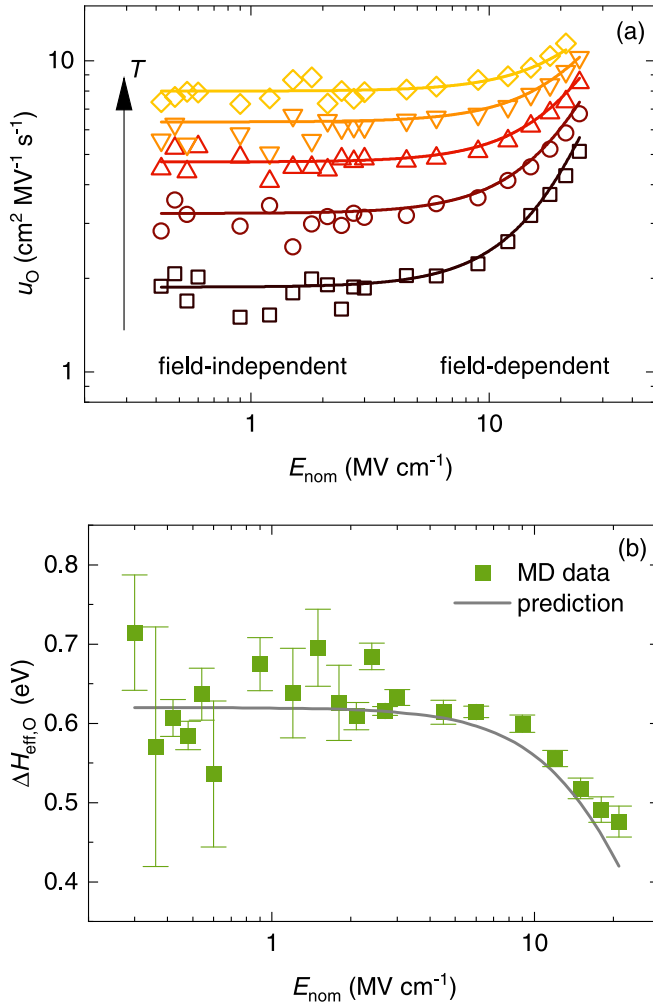


FIG. 2. (a) Oxygen-ion mobility in SrTiO₃, u_O , as a function of nominal field strength E_{nom} (symbols). Data obtained from MD simulations at $T/K = 1500, 1750, 2000, 2250, 2500$. The lines are not fits to the data but predictions from the analytical treatment (see text). (b) Effective activation enthalpy of oxygen-ion mobility as a function of E_{nom} (symbols), obtained from the data shown in (a), compared with the prediction from the analytical treatment.

description of Verwey [11], Frenkel [12], and Mott and Gurney [13].

The quantitative treatment [16] detailed in Sec. II requires only three parameters as input: $\Delta H_{\text{mig},O} = 0.62$ eV and $\nu'_0 = \nu_0 \exp(\Delta S_{\text{mig},O}/k_B) = 4.6$ THz were determined previously in MD simulations of oxygen tracer diffusion with these EPP [28], and $d_O(T) = a_{\text{SrTiO}_3}(T)/\sqrt{2}$ was obtained from the lattice parameter $a_{\text{SrTiO}_3}/\text{\AA} = [3.90 + 6.64 \cdot 10^{-5} (T/K)]$ in this study. The values of $u_O(E, T)$ predicted in this way describe the MD data extremely well, as shown in Fig. 2(a). By describing the data at low fields, the treatment confirms that the Haven ratio needs to be modified by a factor of $(6/Z)$. And by describing the increase in mobility at high fields, the treatment indicates that ignoring the inequivalence of the two migration paths and ignoring the curvature of the migration paths are acceptable approximations. The latter point is confirmed by the good agreement seen in Fig. 2(b) for the effective activation enthalpies. The question then arises of why the

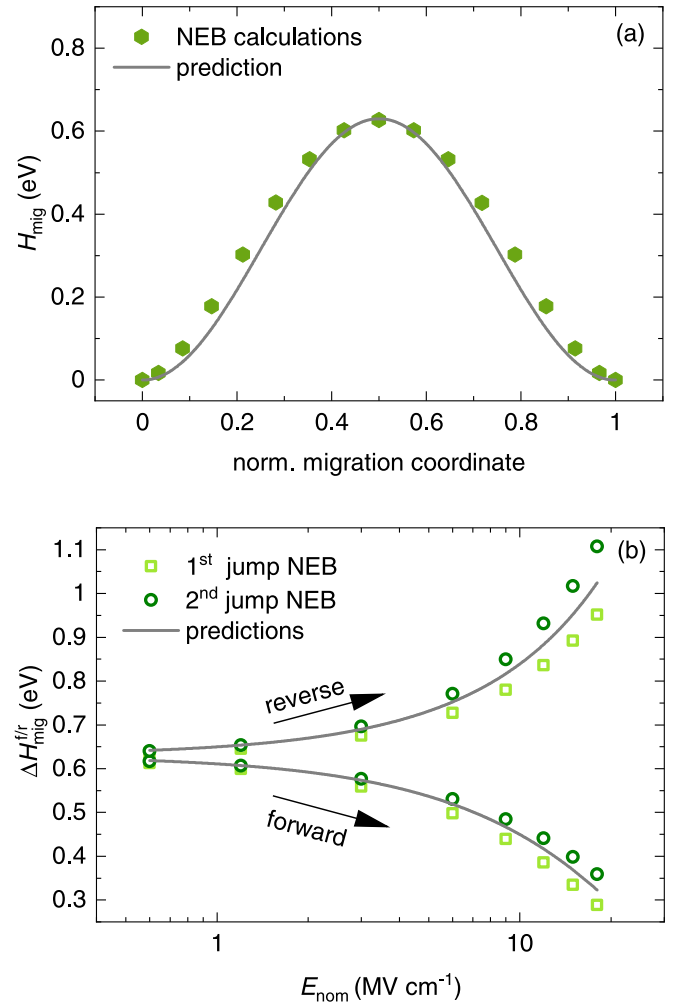


FIG. 3. NEB calculations of oxygen-ion migration by a vacancy mechanism in cubic SrTiO₃. (a) Energy profile along the migration path at zero applied field; the predicted energy profile was calculated with Eq. (2). (b) Activation barriers $\Delta H_{\text{mig}}^{\text{tr}}$ as a function of applied field along $\langle 100 \rangle$. The predicted barriers were calculated with Eq. (3).

treatment works, and this is examined from two sides in the next section.

2. Activation barriers for oxygen-ion migration

Since the quantitative treatment [16] assumes a cosinusoidal shape, the first issue to be examined is the shape of the energy barrier for oxygen-ion migration by a vacancy mechanism. Figure 3(a) shows the energy profile along the migration coordinate obtained by nudged elastic band (NEB) calculations [74] together with the predicted cosinusoidal form [Eq. (2)]. The agreement between the two is rather good. The small positive deviations on the flanks of the NEB profile are attributed, on consideration of Fig. 1(b), to increased Coulomb interactions as the migrating oxygen ion comes closer to neighboring oxygen ions.

Repeating these NEB calculations as a function of applied field yields the data shown in Fig. 3(b). This plot confirms quantitatively that the migration barriers $\Delta H_{\text{mig}}^{\text{tr}}$ are different for the two consecutive jumps, as predicted in Sec. II C, with

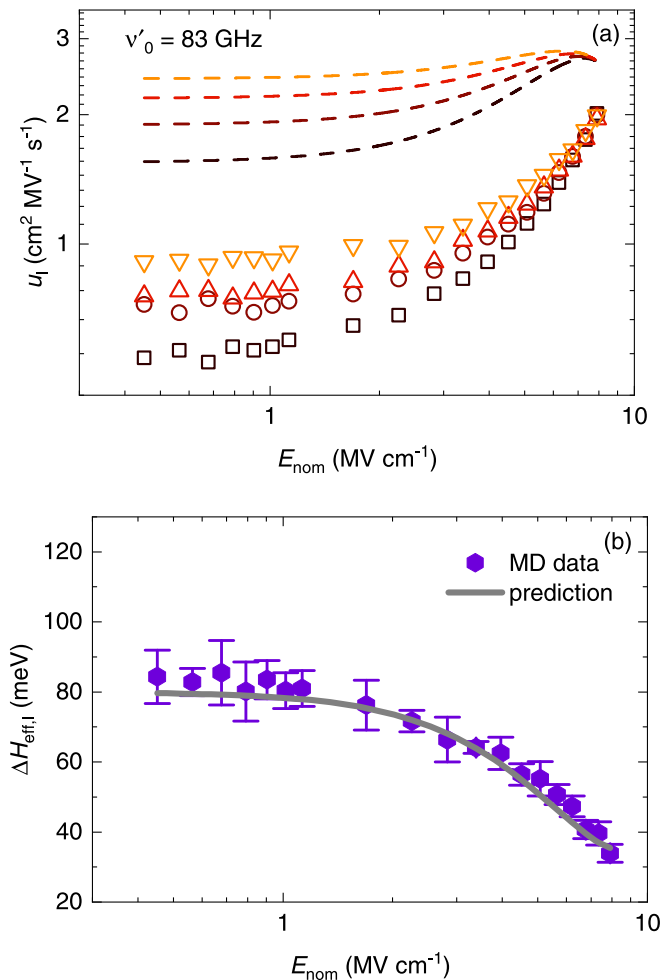


FIG. 4. (a) Iodine ion mobility u_l in $\text{CH}_3\text{NH}_3\text{PbI}_3$ as a function of applied nominal field strength E_{nom} . Data obtained from MD simulations for four different temperatures ($T/\text{K} = 350, 400, 450, 500$) are plotted as symbols. The dashed lines refer to the predicted behavior from the analytical treatment. (b) Effective activation enthalpy of iodine-ion mobility as a function of E_{nom} (symbols), obtained from the data shown in (a), compared with the prediction from the analytical treatment.

the data here revealing that the difference increases with increasing field strength. The plot also confirms that the first forward jump is more strongly affected than the second, and that the first reverse jump is less affected than the second. This behavior can be attributed (see Sec. II C) to the different angles between the field vector and the migration vector. Lastly, the NEB simulations also reveal no perceptible change in migration path, meaning that the ion traces out the same curved migration path even under large E .

Comparing in Fig. 3(b) these NEB data for $\Delta H_{\text{mig}}^{\text{tr}}$ with values predicted with Eq. (3) (the prediction assuming a single barrier affected by a linear superimposed field), we find, remarkably, that the predicted values are the exact average of the two separate NEB values. Closer consideration indicates that this behavior arises because, in the steady state, the flux of ions over each barrier has to be the same. Since the jump rate for an ion crossing the second (higher) barrier is lower than for an ion crossing the first (lower) barrier, there must be

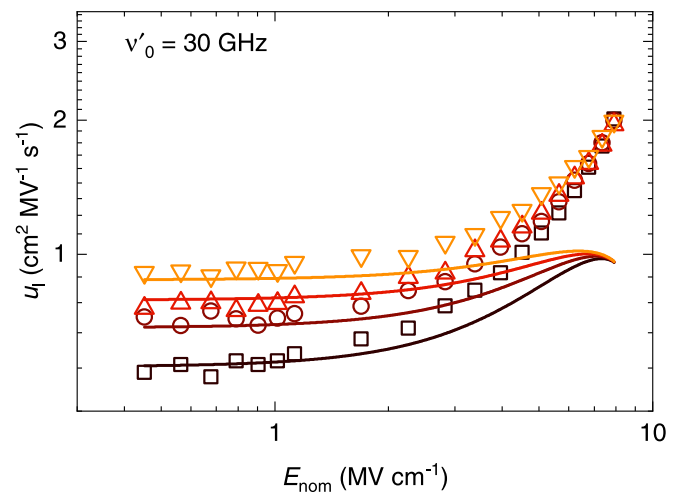


FIG. 5. Description of the low field regime of u_l (symbols) with $v'_0 = 30$ GHz (solid lines) instead of $v'_0 = 83$ GHz. Symbols and lines refer to four different temperatures ($T/\text{K} = 350, 400, 450, 500$).

more ions executing jumps over the second (higher) barrier. In other words, the two sites (before barrier 1 and before barrier 2) have different site occupancies, the exact numbers being a function of the four jump rates (forward and back over first and second barriers).

It thus appears that, at least for a field applied in $\langle 100 \rangle$, the treatment of Sec. II does describe the mobility data effectively because the two barriers are connected in series and the steady state is being considered.

3. Comparison with literature data

Experimental studies [32–34,75,76] of oxygen-ion transport in SrTiO_3 and two related perovskite-type oxides (BaTiO_3 and BiFeO_3) under appreciable applied fields do not provide a coherent picture, as noted in the Introduction. Generally, these studies were performed at or just above room temperature, and hence the field strength above which nonlinear behavior is expected, according to Sec. II and confirmed by our results, is $E \approx (2k_B T)/(|z_i|ed_O) = 0.9 \text{ MV cm}^{-1}$ (for a jump distance of $d_O = 2.8 \text{ \AA}$).

For SrTiO_3 , two of the three studies are consistent with this expectation. Jiang *et al.* [32] examined oxygen-vacancy drift at room temperature under $E = 0.5 \text{ MV cm}^{-1}$ and found no field-enhanced acceleration. Hanzig *et al.* [33] examined vacancy mobility as a function of temperature at $E = 0.01 \text{ MV cm}^{-1}$ and discerned no decrease in activation enthalpy. In contrast, Messerschmitt *et al.* [34] performed experiments only between $0.02 \leq E/\text{MV cm}^{-1} \leq 0.06$ at room temperature, and reported increases in vacancy mobility of one order of magnitude. Since experimental studies of field-accelerated ion transport can be plagued by various problems [14,16,77], we suggest that some other effect produced the changes in mobility reported by Messerschmitt *et al.*

The experiments performed on BaTiO_3 constitute the only study in which field-accelerated oxygen-ion transport is actually evident. Randall *et al.* [76] examined the degradation kinetics of BaTiO_3 -based capacitors—a process governed by the migration of oxygen vacancies—at $0.12 \leq E/\text{MV cm}^{-1} \leq 1.13$ and $307 \leq T/\text{K} \leq 463$. They were able

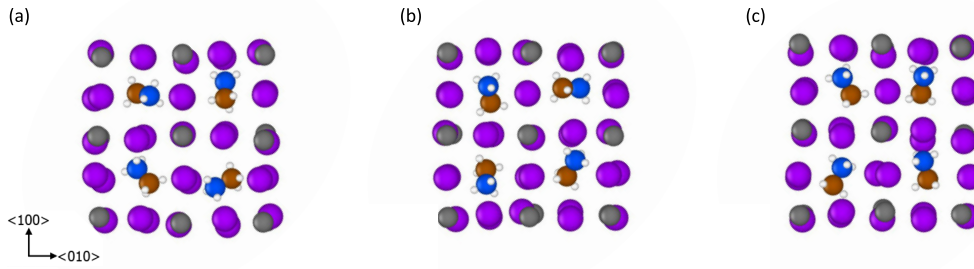


FIG. 6. Snapshots from MD simulations of $\text{CH}_3\text{NH}_3\text{PbI}_3$ at $T = 350$ K and three different field strengths E_{nom} [0.565 MV cm^{-1} (a), 2.26 MV cm^{-1} (b), 6.78 MV cm^{-1} (c)] applied in (100) indicating increased alignment of the methylammonium cations with increasing field. The iodide ions are shown in purple, the lead cations are shown in grey, and the methylammonium cations are shown with nitrogen in blue, carbon in brown, and hydrogen in white.

to describe their entire set of data with a simple sinh-type expression [based on Eq. (1)].

In contrast, the field-driven acceleration of oxygen-vacancy transport invoked in resistive switching studies of BiFeO_3 films [75] requires re-examination because the fields applied are far too low ($E \leq 0.4$ MV cm^{-1}) to produce any noticeable acceleration.

B. Methylammonium lead iodide (MAPbI_3)

The iodine-ion mobility $u_1(E, T)$ obtained from MD simulations as a function of the applied nominal field strength E_{nom} for four different temperatures is plotted in Fig. 4(a). u_1 exhibits field-independent values at low field strengths and nonlinear increases at higher field strengths, analogous to $u_{\text{O}}(E, T)$ for SrTiO_3 [Fig. 2(a)] and qualitatively consistent with the standard description [11–13]. The temperature-dependence gets weaker in the nonlinear regime, and Fig. 4(b) shows quantitatively that the effective activation enthalpy of iodide-ion mobility, $\Delta H_{\text{eff},1} = -k_{\text{B}}[\text{d} \ln(u_1 T)/\text{d}(1/T)]$, decreases in the nonlinear regime, as expected.

To predict $u_1(E, T)$ as described in Sec. II, we took the values $\Delta H_{\text{mig},1} = 80$ meV and $\nu'_0 = \nu_0 \exp(\Delta S_{\text{mig},1}/k_{\text{B}}) = 83$ GHz derived by Barboni and De Souza from MD simulations of iodine tracer diffusion with the same EPP [37]. $d_1(T) = a_{\text{MAPbI}_3}(T)/\sqrt{2}$ was obtained from $a_{\text{MAPbI}_3}/\text{\AA} = [6.23 + 1.97 \times 10^{-4} (T/\text{K})]$. The predicted $u_1(E, T)$ are seen in Fig. 4(a) to overestimate substantially over the entire range of E_{nom} the mobilities obtained from the MD simulations. At low E_{nom} , the predicted temperature dependence appears to be correct (i.e., the relative separation of the individual data sets seems to be the same as that seen for the MD data), even though the predicted values are higher. Indeed, the effective activation enthalpy of iodide-ion mobility can be described quantitatively, as shown in Fig. 4(b), with the analytical treatment using a zero-field barrier of ≈ 80 meV. At high E_{nom} , complex behavior is observed. It appears that $u_1(E, T)$ is not even qualitatively correct [Fig. 4(a)], but $\Delta H_{\text{eff},1}$ is described quantitatively [Fig. 4(b)]. In the following, we consider the low-field and high-field regimes separately.

1. Iodide ion mobilities at low field strengths

Of the three parameters [$\Delta H_{\text{mig},1}$, ν'_0 , and $d_1(T)$] that are required as input for the quantitative treatment, $\Delta H_{\text{mig},1}$ is

evidently correct [cf. Fig. 4(b)] and $d_1(T)$ is unambiguously defined. This leaves ν'_0 as the only parameter that may be modified. As shown in Fig. 5, lowering ν'_0 from 83 GHz to 30 GHz achieves good agreement between the predicted curves and the MD data up to field strengths of just over 1 MV cm^{-1} . This result suggests that applying fields of 0.1 to 1 MV cm^{-1} leads to a reduction in u_1 by a factor of approximately 2.5. Unfortunately, the poor jump statistics at even lower fields prevents us from determining if lower field strengths also produce this effect, i.e., the lower limit for this effect is at present unclear.

Evidence to support a decrease in ν'_0 comes from two recent studies [78,79]. Mattoni and Caddeo [78] examined the rotational dynamics of MA^+ molecules in MAPbI_3 under the influence of an electric field using MD simulations. For $0.01 \leq E/\text{MV cm}^{-1} \leq 0.05$ (and at $T = 326$ K), the MA^+ dipoles were observed to align along the field direction, although strong rotational disorder was still evident due to thermal fluctuations. Our MD simulations confirm that an increase in the dipole alignment occurs, as indicated by the snapshots shown in Fig. 6 and the data shown in Fig. 7. In their static DFT study, Tong *et al.* [79] found that the barrier for iodide-ion migration was higher when the MA^+ dipoles were parallel, compared to when they were antiparallel. Taken together, these results indicate that the probability of having the correct (antiparallel MA^+) molecular arrangement for a successful iodide-ion jump is lowered upon application of a field, because the field tends to line the dipoles up. An iodide ion thus has to wait longer for the lattice to achieve the configuration with the low-energy barrier, and this corresponds to a lower value of ν'_0 . The thermally induced rotational disorder is still sufficiently strong, however, to produce at an adequate frequency the preferred arrangement with the low-energy migration barrier. Consequently, the migration barrier remains at the zero-field value of 80 meV.

It would be desirable to confirm that the energy profile for iodine-vacancy migration in cubic MAPbI_3 has a cosinusoidal form [analogous to the data for SrTiO_3 in Fig. 3(a)]. NEB calculations cannot, however, provide such confirmation because they are static and refer, therefore, to zero Kelvin. At this temperature, the cubic structure of MAPbI_3 is unstable with respect to collective rotations of the PbI_6 octahedra (yielding an orthorhombic structure), and the MA^+ cations are

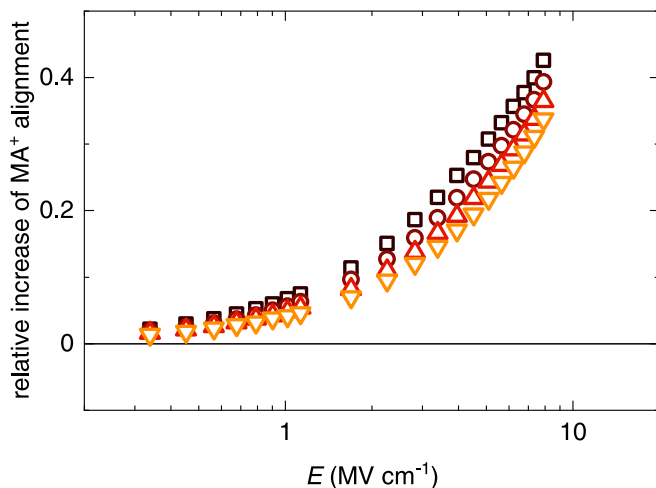


FIG. 7. Relative increase of the alignment of MA^+ cations along the field direction. The alignment is defined as the time-averaged ratio of dipoles pointing in $\langle 100 \rangle$ direction normalized to the ratio at zero field strength. Data refer to the same four different temperatures ($T/\text{K} = 350, 400, 450, 500$).

oriented in specific directions of the perovskite unit cell, rather than rotating freely. Consequently, standard NEB calculations, regardless of whether they are EPP- or DFT-based, will yield incorrect energy profiles (and overestimated activation barriers).

2. Iodide ion mobilities at high field strengths

The high-field behavior is evidently complex. Figure 5 clearly indicates that u_1 is enhanced to a much higher degree than that expected from the analytical treatment. The activation enthalpy for iodine-vacancy migration is not altered, however, from $\Delta H_{\text{mig,I}} = 80$ meV, since the effective activation enthalpy decreases as predicted [Fig. 4(b)] and the breakdown field of the cell is consistent with $\Delta H_{\text{mig,I}} = 80$ meV (see Sec. II A). Furthermore, the increased alignment of the MA^+ dipoles at high fields (Fig. 7) implies that ν'_0 decreases even further, but, since $\Delta H_{\text{mig,I}}$ is correct, ν'_0 has effectively to increase to describe the data. Indeed, one can describe the high-field data with $\Delta H_{\text{mig,I}} = 80$ meV and a field- and temperature-dependent ν'_0 , as shown in Fig. 8. We suggest that the complex behavior arises from the low value of $\Delta H_{\text{mig,I}}$. Under high fields, the forward barrier decreases to the level of $k_B T$. This means that the iodide ions no longer spend most of their time vibrating on their lattice sites, but according to transition-state theory, a substantial proportion of time at the transition state. This effectively gives rise to an increase in ν'_0 that overcompensates for the decrease due to the increased alignment of the MA^+ dipoles. In essence, the analytical treatment is approaching its limits.

3. Comparison with experimental data

At this point, we would have liked to compare our predictions with experimental data. What is required from the experimental side is a full set of $u_1(E, T)$, and such data are not available. In making such measurements, the exper-

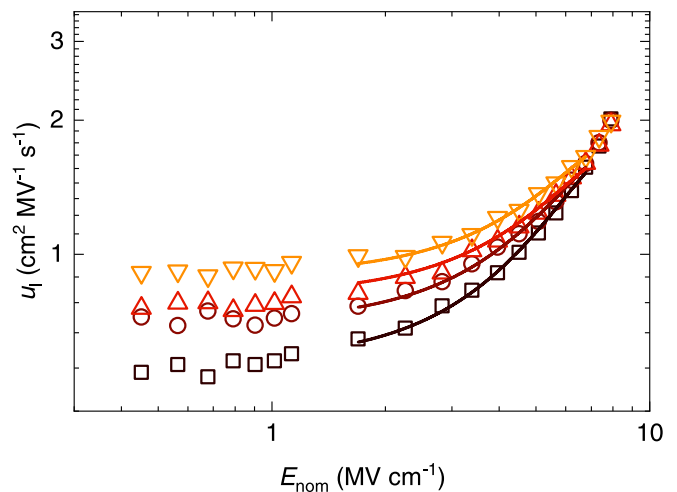


FIG. 8. Description of the high-field regime, $(1.7 - 6.8)$ MV cm^{-1} , with $\Delta H_{\text{mig,I}} = 80$ meV and T - and E -dependent ν'_0 . Symbols and lines refer to four different temperatures ($T/\text{K} = 350, 400, 450, 500$).

imentalist will need to work on single-crystal samples with suitable electrodes (to avoid nonlinear effects from grain boundaries and interfaces) and will need to ensure that iodine-vacancy mobility is being examined, with negligible contributions from iodine interstitials or from methylammonium vacancies [37].

V. EFFECT OF FIELD ON CATION MOBILITY

If one introduces cation vacancies into a simulation cell of SrTiO_3 or MAPbI_3 (this paper, data not shown) {or $(\text{Na}, \text{Bi})\text{TiO}_3$ [50] or LaMnO_3 [52]} to allow cation transport to occur, one observes, even at temperatures close to the melting point, no long-range cation transport. Although the necessary point defects are present, the barriers for cation-vacancy migration are too high [48,80–85] to effect any successful cation jumps on the timescales accessible in MD simulations. (Indeed, if diffusion coefficients are required, one needs to resort to accelerated MD techniques, such as metadynamics [85]).

This is not a problem, however, if one wants to predict field-dependent cation mobilities for the case of the field and migration vectors being collinear and the energy profile for the cation jump having a cosinusoidal form. This is because the treatment given in Sec. II is then directly applicable. Taking strontium-vacancy migration in SrTiO_3 as our example, we find that these two requirements (collinear vectors and a cosinusoidal energy profile) are fulfilled [48,82,83,85] and, hence, the effect of a field on the mobility of Sr ions can be predicted quantitatively with $\Delta H_{\text{mig,Sr}} = 4$ eV, $\nu'_0 = 75.4$ THz and $d_{\text{Sr}}(T) = a(T)$.

In general, field-enhanced rates of ν_A transport in cubic, inorganic ABX_3 perovskites (for fields applied in $\langle 100 \rangle$) can be predicted quantitatively. Given the complex response of the MAPbI_3 lattice to applied fields, we refrain from applying the analytical treatment to MA^+ transport.

VI. CONCLUSIONS

We have obtained the mobility of anions in the ABX_3 structure as a function of field and temperature using classical MD simulations, eluding the problems that generally plague experimental studies. Five points from our study are emphasized.

(1) Our results confirm that for $SrTiO_3$ and $MAPbI_3$, the electric field strength required to enhance anion transport in perovskites is of the order of 10^0 MV cm⁻¹. They also reveal directly ($SrTiO_3$) or indirectly ($MAPbI_3$) that the energy hypersurface for anion migration has a cosinusoidal form.

(2) With knowledge of the activation enthalpy of migration $\Delta H_{\text{mig,O}}$, the effective attempt frequency ν'_0 and the jump distance $d_O(T)$, the oxygen-ion mobility along $\langle 100 \rangle$ in cubic $SrTiO_3$ can be quantitatively predicted as a function of temperature and field strength from an analytical treatment, even though the anions have to jump over two different activation barriers that are affected differently by the field.

(3) If the three quantities are known for other cubic, inorganic ABX_3 perovskite systems, $u_X(E, T)$ can similarly be

predicted. The analytical treatment thus establishes a solid basis upon which experimental results can be judged and with which device behavior can be modeled.

(4) Iodide-ion mobility in cubic $MAPbI_3$ shows complex behavior as a function of temperature and field strength, behavior that is attributed to the interaction of the methylammonium dipoles with the applied field. Moderate fields will lower the iodide-ion mobility.

(5) The standard Haven ratio linking tracer and conductivity diffusion coefficients needs to be modified.

ACKNOWLEDGMENTS

Funding from the German Research Foundation (DFG) within the framework of the collaborative research center Nanoswitches (SFB 917) is acknowledged. Simulations were performed with computing resources granted by RWTH Aachen University under Project No. rwth0441. We thank D. Barboni for performing preliminary calculations.

-
- [1] H. Ogihara, C. A. Randall, and S. Trolrier-McKinstry, *J. Am. Ceram. Soc.* **92**, 1719 (2009).
- [2] H. Kishi, Y. Mizuno, and H. Chazono, *Jpn. J. Appl. Phys.* **42**, 1 (2003).
- [3] G. Catalan and J. F. Scott, *Adv. Mater.* **21**, 2463 (2009).
- [4] D. Sando, A. Barthélémy, and M. Bibes, *J. Phys.: Condens. Matter* **26**, 473201 (2014).
- [5] A. Kojima, K. Teshima, Y. Shirai, and T. Miyasaka, *J. Am. Chem. Soc.* **131**, 6050 (2009).
- [6] M. M. Lee, J. Teuscher, T. Miyasaka, T. N. Murakami, and H. J. Snaith, *Science* **338**, 643 (2012).
- [7] J.-P. Correa-Baena, A. Abate, M. Saliba, W. Tress, T. Jesper Jacobsson, M. Grätzel, and A. Hagfeldt, *Energy Environ. Sci.* **10**, 710 (2017).
- [8] T. Ishihara, H. Matsuda, and Y. Takita, *J. Am. Chem. Soc.* **116**, 3801 (1994).
- [9] K. Szot, R. Dittmann, W. Speier, and R. Waser, *Phys. Status Solidi (RRL)* **1**, R86 (2007).
- [10] S. Menzel, M. Waters, A. Marchewka, U. Böttger, R. Dittmann, and R. Waser, *Adv. Funct. Mater.* **21**, 4487 (2011).
- [11] E. Verwey, *Physica* **2**, 1059 (1935).
- [12] J. Frenkel, *Kinetic Theory of Liquids* (Oxford University Press, Oxford, 1946).
- [13] N. F. Mott and R. W. Gurney, *Electronic Processes in Ionic Crystal*, 2nd ed. (Oxford University Press, Oxford, 1950).
- [14] B. Roling, S. Murugavel, A. Heuer, L. Lühning, R. Friedrich, and S. Röthel, *Phys. Chem. Chem. Phys.* **10**, 4211 (2008).
- [15] A. T. Fromhold and E. L. Cook, *J. Appl. Phys.* **38**, 1546 (1967).
- [16] A. R. Genreith-Schriever and R. A. De Souza, *Phys. Rev. B* **94**, 224304 (2016).
- [17] B. Roling, L. N. Patro, O. Burghaus, and M. Gräf, *Eur. Phys. J.: Spec. Top.* **226**, 3095 (2017).
- [18] J. A. Kilner and R. J. Brook, *Solid State Ion.* **6**, 237 (1982).
- [19] M. Cherry, M. S. Islam, and C. Catlow, *J. Solid State Chem.* **118**, 125 (1995).
- [20] M. S. Khan, M. S. Islam, and D. R. Bates, *J. Phys. Chem. B* **102**, 3099 (1998).
- [21] R. A. De Souza and J. Maier, *Phys. Chem. Chem. Phys.* **5**, 740 (2003).
- [22] M. Lerch, H. Boysen, and T. Hansen, *J. Phys. Chem. Solids* **62**, 445 (2001).
- [23] M. M. Günter, H. Boysen, C. Corte, M. Lerch, and E. Suard, *Z. Krist.-Cryst. Mater.* **220**, 218 (2005).
- [24] A. Hackmann and O. Kanert, *Radiat. Eff. Defects Solids* **119-121**, 651 (1991).
- [25] F. Cordero, *Phys. Rev. B* **76**, 172106 (2007).
- [26] R. A. De Souza, V. Metlenko, D. Park, and T. E. Weirich, *Phys. Rev. B* **85**, 174109 (2012).
- [27] M. Schie, R. Waser, and R. A. De Souza, *J. Phys. Chem. C* **118**, 15185 (2014).
- [28] S. P. Waldow and R. A. De Souza, *ACS Appl. Mater. Interfaces* **8**, 12246 (2016).
- [29] R. A. De Souza, *Adv. Funct. Mater.* **25**, 6326 (2015).
- [30] L. Zhang, B. Liu, H. Zhuang, P. Kent, V. R. Cooper, P. Ganesh, and H. Xu, *Comput. Mater. Sci.* **118**, 309 (2016).
- [31] S. Menzel, M. von Witzleben, V. Havel, and U. Böttger, *Faraday Discuss.* **213**, 197 (2019).
- [32] W. Jiang, M. Noman, Y. M. Lu, J. A. Bain, P. A. Salvador, and M. Skowronski, *J. Appl. Phys.* **110**, 034509 (2011).
- [33] J. Hanzig, M. Zschornak, E. Mehner, F. Hanzig, W. Münchgesang, T. Leisegang, H. Stöcker, and D. C. Meyer, *J. Phys.: Condens. Matter* **28**, 225001 (2016).
- [34] F. Messerschmitt, M. Kubicek, S. Schweiger, and J. L. Rupp, *Adv. Funct. Mater.* **24**, 7448 (2014).
- [35] T.-Y. Yang, G. Gregori, N. Pellet, M. Grätzel, and J. Maier, *Angew. Chem. Int. Ed.* **54**, 7905 (2015).
- [36] A. Senocrate, T.-Y. Yang, G. Gregori, G. Y. Kim, M. Grätzel, and J. Maier, *Solid State Ionics* **321**, 69 (2018).
- [37] D. Barboni and R. A. De Souza, *Energy Environ. Sci.* **11**, 3266 (2018).
- [38] R. A. De Souza and D. Barboni, *Chem. Commun.* **55**, 1108 (2019).
- [39] D. Moia and J. Maier, *ACS Energy Lett.* **6**, 1566 (2021).

- [40] N. Leupold, A. L. Seibel, R. Moos, and F. Panzer, *Eur. J. Inorg. Chem.* **2021**, 2882 (2021).
- [41] S. Menzel, U. Böttger, M. Wimmer, and M. Salinga, *Adv. Funct. Mater.* **25**, 6306 (2015).
- [42] S. Murugavel and B. Roling, *J. Phys. Chem. B* **108**, 2564 (2004).
- [43] A. Stukowski, *Model. Simul. Mater. Sci. Eng.* **18**, 015012 (2010).
- [44] G. E. Murch, *Solid State Ion.* **7**, 177 (1982).
- [45] G. E. Murch and J. C. Dyre, *Crit. Rev. Solid State Mater. Sci.* **15**, 345 (1989).
- [46] T. Ishigaki, S. Yamauchi, K. Kishio, J. Mizusaki, and K. Fueki, *J. Solid State Chem.* **73**, 179 (1988).
- [47] J. B. Goodenough, *Annu. Rev. Mater. Res.* **33**, 91 (2003).
- [48] V. Metlenko, A. H. H. Ramadan, F. Gunkel, H. Du, H. Schraknepper, S. Hoffmann-Eifert, R. Dittmann, R. Waser, and R. A. De Souza, *Nanoscale* **6**, 12864 (2014).
- [49] J. P. Parras, A. R. Genreith-Schriever, H. Zhang, M. T. Elm, T. Norby, and R. A. De Souza, *Phys. Chem. Chem. Phys.* **20**, 8008 (2018).
- [50] H. Zhang, A. H. H. Ramadan, and R. A. De Souza, *J. Mater. Chem. A* **6**, 9116 (2018).
- [51] H. Zhang and R. A. De Souza, *J. Mater. Chem. A* **7**, 25274 (2019).
- [52] J. M. Börgers and R. A. De Souza, *Phys. Chem. Chem. Phys.* **22**, 14329 (2020).
- [53] S. Grieshammer, B. O. H. Grope, J. Koettgen, and M. Martin, *Phys. Chem. Chem. Phys.* **16**, 9974 (2014).
- [54] J. Koettgen, S. Grieshammer, P. Hein, B. O. H. Grope, M. Nakayama, and M. Martin, *Phys. Chem. Chem. Phys.* **20**, 14291 (2018).
- [55] F. M. Draber, C. Ader, J. P. Arnold, S. Eisele, S. Grieshammer, S. Yamaguchi, and M. Martin, *Nat. Mater.* **19**, 338 (2020).
- [56] A. Pedone, G. Malavasi, M. C. Menziani, A. N. Cormack, and U. Segre, *J. Phys. Chem. B* **110**, 11780 (2006).
- [57] J. Kaub, J. Kler, S. C. Parker, and R. A. De Souza, *Phys. Chem. Chem. Phys.* **22**, 5413 (2020).
- [58] A. Mattoni, A. Filippetti, M. I. Saba, and P. Delugas, *J. Phys. Chem. C* **119**, 17421 (2015).
- [59] A. Mattoni, A. Filippetti, and C. Caddeo, *J. Phys.: Condens. Matter* **29**, 043001 (2017).
- [60] C. Caddeo, A. Filippetti, and A. Mattoni, *Nano Energy* **67**, 104162 (2020).
- [61] P. Delugas, C. Caddeo, A. Filippetti, and A. Mattoni, *J. Phys. Chem. Lett.* **7**, 2356 (2016).
- [62] H. Hirao, H. Chen, M. A. Carvajal, Y. Wang, and S. Shaik, *J. Am. Chem. Soc.* **130**, 3319 (2008).
- [63] M. Calvaresi, R. V. Martinez, N. S. Losilla, J. Martinez, R. Garcia, and F. Zerbetto, *J. Phys. Chem. Lett.* **1**, 3256 (2010).
- [64] H. J. Kreuzer, *Surf. Interf. Anal.* **36**, 372 (2004).
- [65] S. Ciampi, N. Darwish, H. M. Aitken, I. Díez-Pérez, and M. L. Coote, *Chem. Soc. Rev.* **47**, 5146 (2018).
- [66] F. Che, J. T. Gray, S. Ha, N. Kruse, S. L. Scott, and J.-S. McEwen, *ACS Catal.* **8**, 5153 (2018).
- [67] A.-M. El-Sayed, M. B. Watkins, T. Grasser, and A. L. Shluger, *Phys. Rev. B* **98**, 064102 (2018).
- [68] S. Plimpton, *J. Comput. Phys.* **117**, 1 (1995).
- [69] P. P. Ewald, *Ann. Phys.* **369**, 253 (1921).
- [70] R. W. Hockney, *Computer Simulation Using Particles* (CRC Press, Boca Raton, 1988).
- [71] S. Nosé, *J. Chem. Phys.* **81**, 511 (1984).
- [72] W. G. Hoover, *Phys. Rev. A* **31**, 1695 (1985).
- [73] M. Schie, S. Menzel, J. Robertson, R. Waser, and R. A. De Souza, *Phys. Rev. Mater.* **2**, 035002 (2018).
- [74] G. Henkelman, B. P. Uberuaga, and H. Jónsson, *J. Chem. Phys.* **113**, 9901 (2000).
- [75] N. Du, N. Manjunath, Y. Li, S. Menzel, E. Linn, R. Waser, T. You, D. Bürger, I. Skorupa, D. Walczyk, C. Walczyk, O. G. Schmidt, and H. Schmidt, *Phys. Rev. Appl.* **10**, 054025 (2018).
- [76] C. A. Randall, R. Maier, W. Qu, K. Kobayashi, K. Morita, Y. Mizuno, N. Inoue, and T. Oguni, *J. Appl. Phys.* **113**, 014101 (2013).
- [77] I. Valov and W. D. Lu, *Nanoscale* **8**, 13828 (2016).
- [78] A. Mattoni and C. Caddeo, *J. Chem. Phys.* **152**, 104705 (2020).
- [79] C.-J. Tong, W. Geng, O. V. Prezhdo, and L.-M. Liu, *ACS Energy Lett.* **2**, 1997 (2017).
- [80] R. Meyer, R. Waser, J. Helmbold, and G. Borchardt, *Phys. Rev. Lett.* **90**, 105901 (2003).
- [81] K. Gömann, G. Borchardt, M. Schulz, A. Gömann, W. Maus-Friedrichs, B. Lesage, O. Kaïtasov, S. Hoffmann-Eifert, and T. Schneller, *Phys. Chem. Chem. Phys.* **7**, 2053 (2005).
- [82] A. Walsh, C. R. A. Catlow, A. G. H. Smith, A. A. Sokol, and S. M. Woodley, *Phys. Rev. B* **83**, 220301(R) (2011).
- [83] T. Mizoguchi, N. Takahashi, and H.-S. Lee, *Appl. Phys. Lett.* **98**, 091909 (2011).
- [84] U. N. Gries, M. Kessel, F. V. E. Hensling, R. Dittmann, M. Martin, and R. A. De Souza, *Phys. Rev. Mater.* **4**, 123404 (2020).
- [85] H. J. Heelweg and R. A. De Souza, *Phys. Rev. Mater.* **5**, 013804 (2021).